Article citation info:
Bober B, Andrych-Zalewska M, Boguś P. Influence of exhaust manifold modification on engine power. Combustion Engines. 2024;196(1):54-65. https://doi.org/10.19206/CE-171389

Bartosz BOBER
Monika ANDRYCH-ZALEWSKA
Piotr BOGUŚ

Combustion Engines
Polish Scientific Society of Combustion Engines

Influence of exhaust manifold modification on engine power

ARTICLE INFO

Received: 20 April 2023
Revised: 5 June 2023
Accepted: 19 August 2023
Available online: 7 September 2023

The article deals with the subject of the impact of an exhaust system on the power of the internal combustion engine. In particular the article shows the possibility of increasing the power of the gasoline drive unit, interfering only with an exhaust system. The purpose of the tests carried out is to compare the results of measurements from the chassis dynamometer before and after the modification, and additionally to perform simulations for the key parts of the system in terms of shaping the power and torque curves. The analysis includes a simulation model of the exhaust gas flow through the serial manifold and also the sport manifold, especially the pressure distribution and the course of the velocity vectors at the characteristic points of the element. Before obtaining the final results of power measurements on the sport units, the roughness of the steel from which the collectors were made was also measured. The final stage is the measurement of power on the new exhaust system. The obtained results of power measurements and simulations were presented in the form of a summary, which focused on the impact of individual fluid mechanics phenomena on the formation of power and torque curves and detailed the advantage of the new exhaust system in comparison with the factory system in terms of increasing the performance of the tested vehicle.

Key words: *exhaust manifold, engines, CFD*

1. Introductions

The constructions of internal combustion engines commonly used in the automotive industry consist of many interdependent systems that affect the final use of the vehicle. Taking into account the internal combustion engine, through power transmission systems, braking systems, suspension systems, steering systems, or exhaust systems discussed in more detail in this work. So many systems involved in the conversion of thermal energy into mechanical energy contribute to the formation of a significant number of potential energy loss centers and thus give an opportunity for optimization of individual systems in order to increase the performance of the entire vehicle [7].

The impact of the exhaust system on the engine's operating indicators is an aspect that, along with the development of the automotive industry, has become particularly important in terms of optimizing vehicle performance. This significantly complicated the stage of designing the exhaust systems, because it has a decisive impact on the efficiency of exhaust gas removal, which ultimately translates into the nature of the torque curve as a function of engine speed. Initially, this condition was somewhat inconsistent with maintaining normative noise levels (acoustic silencers effectively inhibited the flow of exhaust gases, which led to their less effective removal and thus to a reduction in the power generated by the engine). Over some time, the interest started to focus on finding a compromise between noise suppression and maximizing vehicle performance, which was, among other, the reason for the creation of various silencer designs. In a situation where, however, we focus on increasing the performance itself, expanding and separating dampers should be used. This solution ensures free expansion of the gas (reducing the energy of the sound wave) and thus by separating the flue gas column by a bundle of parallel pipes with small cross-sections will help to avoid too much throttling of the flow (very advantageous in terms of increasing power). As a result of such a solution, we will not disturb the effective exhaust gas flow and ensure sufficient damping [12, 13].

However, the sound pressure generated in the exhaust system can be used to maximize engine performance. After opening the exhaust valve, the exhaust gases coming out of the combustion chamber will generate the so-called "reflection" of pressure pulses. The returning vacuum wave flowing into the cylinder while a piston approaches the bottom dead center (intake valve opening) will purge the chamber of exhaust gas and accelerate the intake cycle at the same time. The choice of the co-opening stage of the valve will result in more effective filling of the cylinder and almost complete exhaust gas removal. However, this may result in some unburned mixture entering the exhaust pipe, which will certainly increase fuel consumption. This phenomenon is commonly used in sports cars, where they are additionally equipped with structurally matched camshafts, which are to ensure the extension of the valve co-opening interval and thus increase the probability that the negative vacuum wave will ensure more effective cylinder filling [12–14].

2. Literature review

Exhaust manifolds collect exhaust gases from the engine cylinders and release them into the atmosphere through the exhaust system. Engine efficiency and combustion characteristics depend on the method of exhaust gas removal from the cylinder. The design of the exhaust manifold for an internal combustion engine depends on many parameters, such as. exhaust back pressure, exhaust velocity, etc. [11] The exhaust manifold affects emission efficiency and fuel economy, which is why its proper sizing is so important.

The authors of the publication [18] designed the original and modified X-shaped system model using Catia software and then analyzed them using CFD software in terms of

flow velocities and temperature distribution in the exhaust gas models. The best modification was determined.

The subject of manifold modifications was also addressed in the publication [4], where the exhaust manifold was redesigned by determining the thermal stresses and deflections occurring under various working conditions with different materials and temperatures. The article aimed to ensure the suitability of the design for a specific material from the point of view of reliability and usability. Existing multiple defects include cracks that typically occur due to prolonged exposure to temperature extremes, casting defects, and repeated thermal cycling. Weld areas and curved profiles are critical failure areas. A methodology has been developed to ensure the best adaptation of the structure and material to the given working conditions. The different behavior of cast iron was analyzed. By redesigning the curved profiles, the impact of fumes on the welds can be reduced. Creo 3.0 software was used to prepare the CAD model of the 4–1 exhaust manifold.

In the investigations [3], the operation of the exhaust manifold of a four-stroke four-cylinder gasoline engine when using three types of fuel (gasoline, methane and methanol) was analyzed to estimate the characteristics of flow and back pressure. Modeling is done in Fluent 18.0, followed by analysis and meshing in ANSYS. Velocity, pressure and temperature profiles were run at an engine speed of 1000 rpm. It was found that methanol provided the highest exit temperature and back pressure, while methane provided the lowest exit pressure. Back pressure decreased while using gasoline. Methane resulted in the best exhaust manifold performance.

The design geometry of the exhaust manifold plays an important role in the smooth combustion and emission reduction of a gasoline engine. In the publication [24], by analyzing and comparing the exhaust back pressures and their speeds of different types of manifold models selected for different engine operating load conditions, the best model 5 exhaust manifold was found and its use in a multipurpose cylinder engine was for engine emission control and environmental protection recommended. The analysis is carried out with a virtual manifold model. The modeling and analysis of the exhaust manifold is done with the software CATIA v5 and ANSYS.

The article [21] discusses the challenges associated with the transformation of the existing multi-cylinder diesel breather system into an innovative monolithic collector model. Reaction gases after cleaning car engines are increasingly used for the benefit of environmental quality, especially in a large metropolitan area of the country, using exhaust systems to eliminate their main pollutants. A well-conditioned exhaust system increases engine performance. The efficiency of the collector has a significant impact on the performance of the engine. With the accelerated development of modern technologies and numerical methods, computer simulation has become a valuable method for research and development of fluid flow systems. Industrial CFD software was used to analyze the exhaust manifold system. In order to expand the basic understanding of diverse processes, extensive knowledge about the distribution of flow and heat transfer properties was gained. Calculations were performed to examine the parametric effect of operating conditions and mathematics on manifold exposure. Suggestions were made to improve the complex plan and execution.

The aim of the work [15] is to analyze the operation of the engine exhaust manifold. This is because the engine's exhaust manifold is a key factor in engine performance. In this work, the distributor design is created with CAD software and analyzed with ANSYS. This CFD analysis and thermal analysis were also performed to verify the performance of the redesigned exhaust manifold. The purpose of the CFD simulations carried out is to investigate the behavior of the volumetric exhaust gas efficiency.

The article [11] presents the latest research [5, 8–10, 22, 23, 25] on exhaust manifold design, evaluation of its operation with experimental methods, and collection and discussion of numerical methods (CFD), different geometry types of exhaust manifolds and their impact on performance.

3. Research methodology

3.1. Research object

The object of research in the conducted experiment is a vehicle with a factory exhaust system, except for the end silencer, which was custom-made to the dimensions of factory exhaust pipes. The material from which the silencer was made is stainless steel 304. Due to the small impact of the final silencer itself on the power of the tested engine, we assume that the exhaust system before modification is fully serial. The vehicle was also modified in the form of replacing the engine with a unit with a larger capacity than the factory one. All transmission systems such as gearbox, propeller shaft, axle shafts and differential have remained unchanged. The factory exhaust manifold is shown in Fig. 1 and 2.

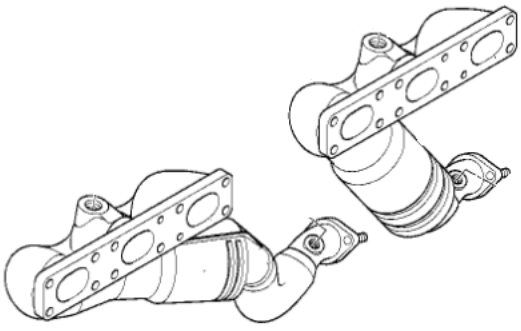

Fig. 1. Factory exhaust manifolds [19]

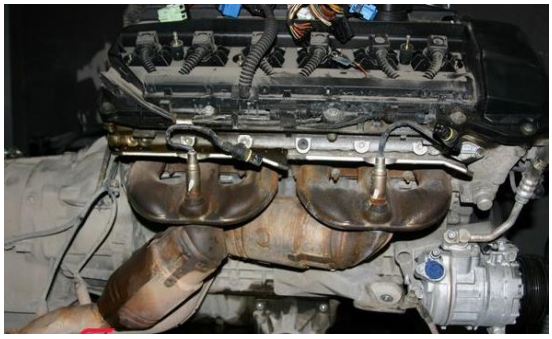

Fig. 2. Factory manifolds mounted on the engine

Table 1. Parameters of the tested vehicle

Stroke capacity [cm^3]	2979
Power* [HP]	231
Torque* [Nm]	300
Acceleration* 0–100 [km/h]	6.9
Yearbook	2003
Course [km]	290 000
Fuel consumption in the combined cycle* [l/100 km]	9.6
Fuel consumption in city driving* [l/100km]	13.4
Fuel consumption on the road* [l/100km]	7.3
*Parameters such as: power, torque, acceleration and fuel consumption are catalogue parameters presented by the manufacturer and due to the mileage of the vehicle they may differ from the actual measurement results from the dynamometer.	

3.2. Chassis dynamometer test bed

The power measurement was carried out on the MAHA LPS 3000 chassis dynamometer test bed at the Wroclaw University of Technology. The LPS 3000 consists of:

– communicating desktop with PC, monitor and mouse
– remote control
– roller set.

The dynamometer is equipped with a rotational speed sensor, an oil temperature sensor, an exhaust gas temperature sensor, a fan, and a junction box. The range of rotations that can be measured is: 0–10,000 rpm, with a measurement accuracy of 2%. Load simulation is carried out using an eddy current brake. The LPS 3000 test bad allows you to measure the power of petrol, gas and diesel engines. The use of an appropriate roller set and electronic system allows for measurements of 4-wheel drive vehicles. More detailed specifications of the research setup have been compiled in Table 2 [16].

Before the measurement, the tire pressure level in the vehicle was checked; all driving assistance systems (two-stage DSC system), and air conditioning were turned off and the maximum airflow was turned on to switch the cooling system into a circuit that included an additional fan. The view of the vehicle on the measuring stand is shown in Fig. 3.

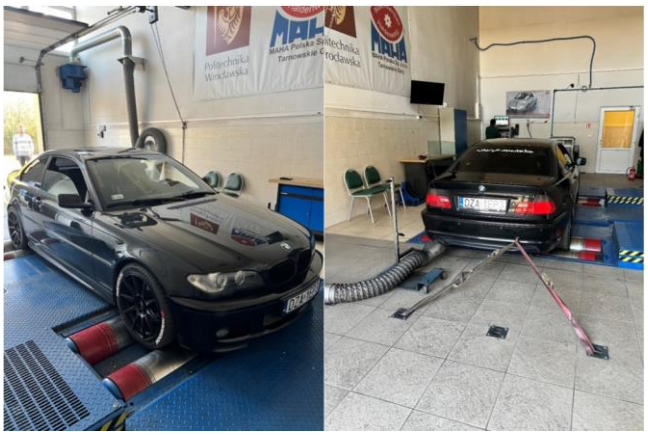

Fig. 3. View of the test stand

Table 2. MAHA LPS 3000 specifications

	R50	R100/1	R100/2	R200/1	R200/2
Roller Set					
Length [mm]	1420	3345	4140	4550	2260
Width [mm]	1100	1100	1100	1100	1100
Height [mm]	505	520	520	570	800
Weight incl. packing	550 kg	1400 kg	1700 kg	2500 kg	2800 kg
Axle load	1.5 t	2.5 t	2.5 t	15 t	15 t
Roller length	220 mm	750 mm	750 mm	900 mm	900mm
Track min.		800 mm	800 mm	820 mm	950 mm
Track max.		2300 mm	2300 mm	2620 mm	2750 mm
Smallest testable wheel	12″	12″	12″	12″	12″
Roller diameter	318 mm	318 mm	318 mm	318 mm	318 mm
Roller axle separation	560 mm	540 mm	540 mm	565 mm	565 mm
Lifting Bar					
Pneumatic	min. 5 bar max. 8 bar	min. 5 bar max. 8 bar	min. 5 bar max. 8 bar		
Hydraulic				up to max. 40 bar	up to max. 40 bar
Electrical Data					
Eddy current brake	260 kW	260 kW	2 × 260 kW	2 × 260 kW	2 × 260 kW
Power supply	230 V/ 50 Hz	230 V/ 50 Hz	230 V/ 50 Hz	400 V/ 50 Hz	400 V/ 50 Hz
Fuse	16 A slow	16 A slow	35 A slow	35 A slow	63 A slow
Display Range					
Test speed	max. 300 km/h	max. 260 km/h	max. 260 km/h	max. 200 km/h	max. 200 km/h
Wheel power	max. 260 kW	max. 260 kW	max. 520 kW	max. 400 kW	max. 600 kW
Traction	max. 6 kN	max. 6 kN	max. 12 kN	max. 15 kN	max. 25 kN
Measurement accuracy	± 2%	± 2%	± 2%	± 2%	± 2%

4. Flow simulation

4.1. Serial collector

Due to the complexity of the calculations and the difficulty in measuring the entire system, the flow analysis will only include calculations for both collectors (before and after the modification). The model of the serial collector was made in the Autodesk Inventor environment (Fig. 4). The collector model has been simplified so that it contains only the nephralgic points of the structure. Autodesk Inventor is a high advanced software 3D to make projects of mechanical elements. The design was made in Inventor. The finished model was exported in the STEP format to the Ansys program, where exhaust gas flow simulations were performed.

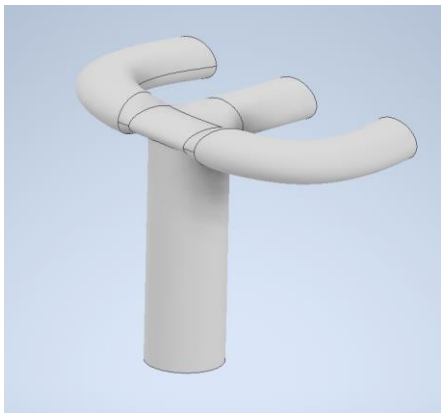

Fig. 4. Model of serial collector (designed in Autodesk Inventor)

By comparing the prepared model with the actual geometry of the collector, it becomes evident that a catalyst is positioned just after the channel that connects all the outputs. However, owing to the complexity of calculations and the aim to solely highlight the impact of collector geometry on computational analysis, the catalyst was omitted. Moreover, the extension of the output channel was undertaken to stabilize simulation results upon exiting the connector. This research was grounded in a comparative analysis of two collector geometries, with the goal of elucidating the effects of geometric disparities on flow resistances, subsequently leading to losses in exhaust evacuation efficiency. In line with these premises and to simplify the factory collector model's design (excluding the catalyst's influence from the analysis), a section right after the convergence of the three channels was represented as a straight pipe. This decision stemmed from the area's limited influence on final analysis outcomes; primary flow losses occur where the pipes assume curvilinear shapes. The first step in the analysis was to determine the consistency of the model geometry. The program correctly read the converted format, so the next step was to generate the mesh. The purpose of the following analysis was to establish, in a comparative manner, the superiority of employing a sports collector over a factory collector. The CFD simulation was also rooted in a comparative study design, leading to the adoption of mesh size and quantity at consistent levels, which were justified by the substantial influence of mesh resolution on the study outcomes.

Consequently, mesh refinement was implemented in potentially significant regions for analysis (high accuracy meshing was applied to areas directly adjacent to pipe walls, where the flow of exhaust gases undergoes rapid changes in direction and velocity). These regions were categorized into a boundary layer and a central layer. Introducing excessive variability in mesh refinement would raise concerns about inaccuracies in results due to disparities between precise and less precise outcomes. This, in turn, could lead to a misconstrued interpretation of flow behavior, challenges in achieving a stable numerical equilibrium state, prolonging the simulation process, or even impeding its completion. Moreover, countermeasures were taken to mitigate turbulence and to preclude the program from autonomously interpolating unstable mesh regions.

In accordance with the aforementioned premises and the comparative nature of the entire study, boundary conditions were established.

The parameterization was carried out automatically, and in order to increase the accuracy on the boundary layer, the "Inflation" function was used (parameters are shown in Table 3), which allows you to create a zone of directional compaction on the selected volume [1, 2, 7, 17]. The compaction value was defined by determining the height of the first layer, which was 0.0001 m, the rest of the value was left unchanged. The grid of the collector model is shown in Fig. 5. The determination of ultimate parameters was preceded by iteratively conducting simulations for different values. The selection rationale was grounded in the program's relatively modest computational demand and the satisfactory precision of research findings.

Table 3. Assumed parameter values in the "Inflation" function

Scope	
Scoping method	Geometry selection
Geometry	1 body
Definition	
Suppressed	No
Boundary scoping method	Geometry selection
Boundary	13 faces
Inflation option	First layer thickness
First layer height	0.001 m
Maximum layers	5
Growth rate	1.2
Inflation algorithm	Pre

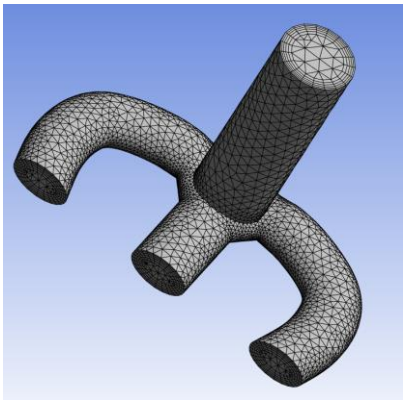

Fig. 5. Grid of the serial collector model

The next stage of the simulation is to determine the boundary conditions that will simplistically represent the tested flow. The nature of the flue gases leaving the combustion chamber and the geometry of the collector affect the lack of identity between the parameters of individual gas molecules, so the computational model assumes the presence of turbulent flow [1]. The material from which the serial collector was made is not known, and the simulation itself concerns the influence of geometry at the given input parameters, therefore the material of the model is steel, while the substance that will imitate the fuel combustion product is air. The next stage of determining the boundary conditions was to determine the places of inlet and outlet of the gas stream by assigning an appropriate function to the previously named walls. The purpose of the following analysis was to establish, in a comparative manner, the superiority of employing a sports collector over a factory collector. As a result, computations were carried out under uniform conditions. The selection of the inlet gas velocity was set at 200 m/s, and its value does not reflect the actual gas emanating from the engine chamber. Nevertheless, the order of magnitude closely approximates the existing conditions in internal combustion engines. The calculations were carried out for the number of iterations equal to 200.

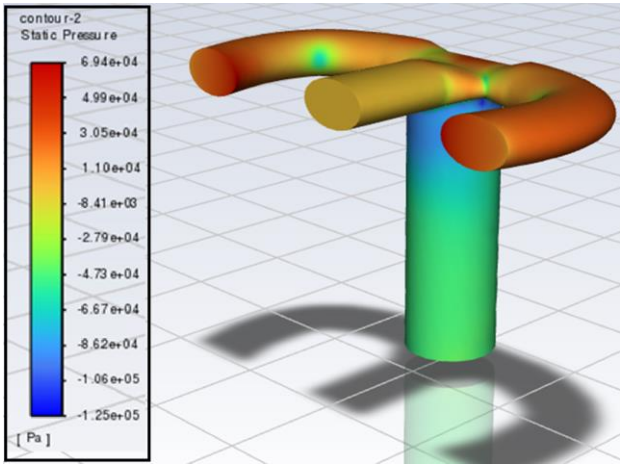

Fig. 6. Pressure distribution on the manifold walls

The simulation result, shown above, presents the distribution of pressure exerted on the manifold walls by the flowing gas stream. The geometry of the collector contributes to a significant variation in the level of pressure values achieved. Considering the model as divided into two parts, we can specify the area in which the pipe channels led from the engine block allow the flow of exhaust gases in the horizontal plane and the area in which, after connecting the individual pipes, the flow takes place in the vertical plane. In the first area, the pressure inside the system builds up, the exhaust gases coming out of the exhaust valve, in the case of cylinders one and three or four and six, are forced by the geometry of the manifold to change the flow direction by 90 degrees. Despite the gentle rounding of the channels, these areas are the zones of the greatest gas pressure on the walls of the considered element and thus will be potential centers for generating the largest energy losses in the flow. Observing the second part of the conventional division of the collector model, where the flue gas again is forced to change the flow direction by the value of a right angle, and the individual channels merge into one pipe, one can notice a huge difference in the pressure inside. This is the area where the flow resistance will be lower, and such a high pressure drop will probably increase the efficiency of mixing streams from individual channels. The results of the simulation of pressure distribution on the walls of a standard collector are shown in Fig. 6.

4.2. Sports collector

The model of the sports manifold was also made in Autodesk Inventor, and then converted in the STEP format to Ansys 2022. In the case of the new system, the catalyst was a separate element, which is located further down, while the exhaust channel, as in the previous manifold, was extended. The collector model is shown in Fig. 7.

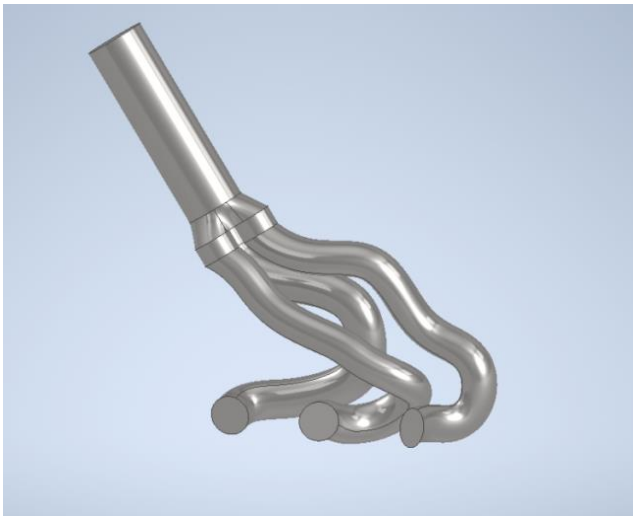

Fig. 7. Sport collector model (Autodesk Inventor)

The stage of creating the model mesh was the same as in the case of the serial collector, for the same values of the boundary layer density. The boundary conditions in this case also took into account the turbulent nature of the gas flow, the material was steel, while the inlet velocity was Vi = 200 m/s and was carried out by the adopted gas, i.e. air. The calculations were also carried out for the number of iterations of 200. The mesh model is shown in Fig. 8.

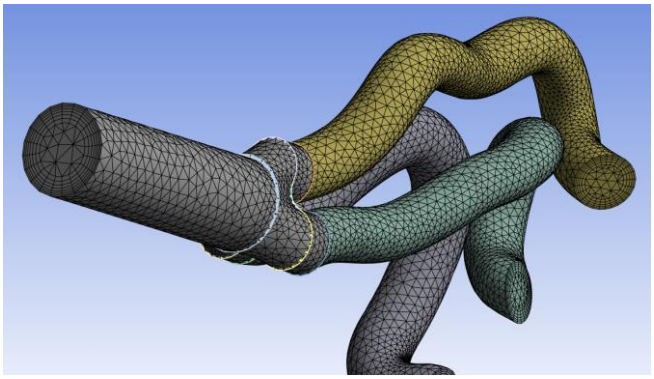

Fig. 8. Grid of the sports collector model

Figure 9 shows the local extremes in the pressure course on the considered geometry. It can be seen that the highest values occur right at the flue gas inlet to the collector, which is probably due to the shape of the pipe, which with its numerous bends is not conducive to free flue gas outflow. The main centers of maximum pressure are located on the outer walls of the bent pipe, where the flow of fluid as it exits the engine, in the direction normal to the outlet port, is reflected from the inside of the manifold, causing a sudden change in flow direction. Such a scenario results in a high pressure of the dynamically flowing exhaust gases on the pipe wall and thus generates an increase in flow resistance. The focus of the maximum pressure in the model will probably also be the place of maximum resistance in the outflow of exhaust gases from the engine.

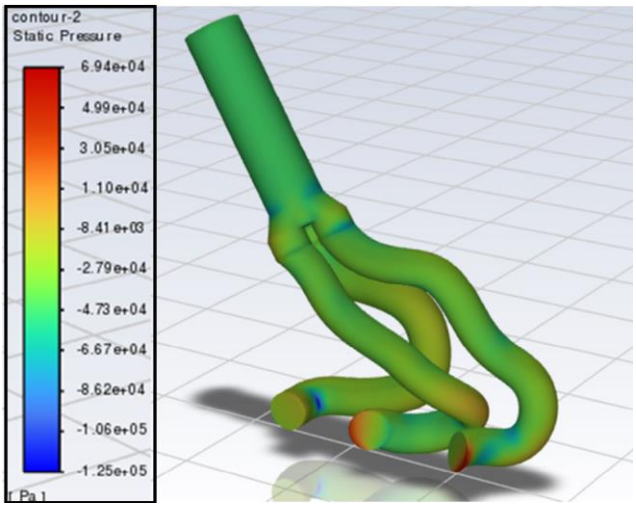

Fig. 9. Distribution of pressures on the collector walls and flow velocity in the sports collector

5. Roughness analysis

In order to check and compare the surface of steel from which the individual systems are made, the roughness measurement of material samples from the factory manifold and the sports manifold was carried out. The examination was performed using the PHENOM X-PRO scanning microscope for 500–2000x magnification. Before the measurement, the samples of individual steels were thoroughly cleaned and degreased and then mounted on the appropriate test table. In order to increase the reliability of the test, the roughness was measured in three different areas and for five different reference lines in each area.

The carried out roughness measurements show a measurable degree of unevenness for both tested steels. The increased amount of unevenness of the inner surface of the steel pipe will directly translate into an increase in the resistance to movement of the flowing gas in the area of the boundary layer. It should be noted that the first steel sample was cut from a previously used factory manifold, so any contamination and wear from a previous use will affect the roughness.

The values of the R_a and R_z roughness parameters are given in μm and are a kind of averaged roughness value. R_a differs from R_z in the method of measuring and calculating the parameter value. Taking into account the profile as the function y on mean line distance x R_a parameter is define as

$$R_a = \frac{1}{l}\int_A^B |y|dz \approx \frac{1}{n}\sum_{i=1}^{n}|y_i| \quad (1)$$

and describes arithmetic mean of absolute values of deviation between observed profile and mean line on the elementary interval in l length (in practice this is calculated as the sum absolute values of successive values of profile y_i in l length). In turn R_z parameter is define as

$$R_z = \frac{1}{5}\left(\sum_{i=1}^{5}|y_{pi}| + \sum_{i=1}^{5}|y_{vi}|\right) \quad (2)$$

and describes arithmetic mean of absolute values of five highest altitudes and five lowest valleys heights of observed roughness profile on the elementary interval in l length.

The higher the value of the parameter, the greater the roughness (larger scratches and surface irregularities). If $R_a > 12.5$, the surface is considered to have high roughness, R_a between 10 and 1.25 is medium roughness, and $R_a < 1.25$ is low roughness (high surface smoothness). The mirror-look steel surface is R_a less than 0.2 [6].

The test result effectively details the advantage of the steel used for the production of the sports manifold, where, according to the R_a parameter, the average roughness of the second steel is lower by 3.26 μm, while in relation to the R_z parameter, this difference will be as much as 11 μm. Differences in roughness values for individual coefficients result from the nature of their determination. To determine the degree of unevenness according to the R_a parameter, the values of deviations on the section specified by Polish standards are read, while to determine the degree of roughness R_z, the five largest elevations and five largest holes on the surface should be measured. A clear difference in the R_z values indicates a high amplitude of surface irregularities for the steel used for the serial collector.

The measurement results for the standard collector are shown in Fig. 10, 11 and in Table 4. The measurement results for the modified collector are shown in Fig. 12, 13 and in Table 5.

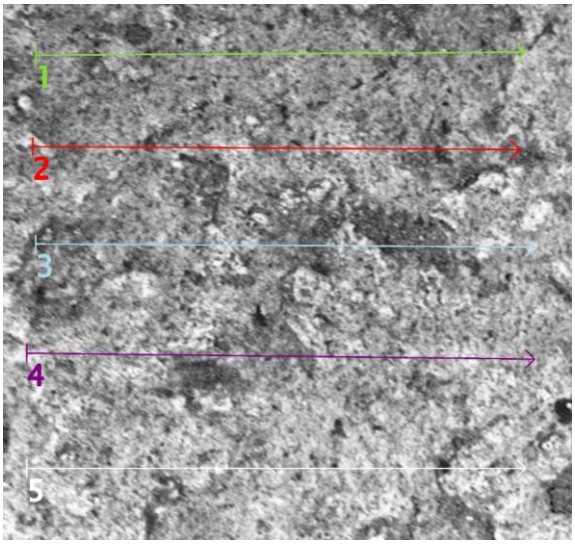

Fig. 10. Surface of a steel sample from a serial collector (2D)

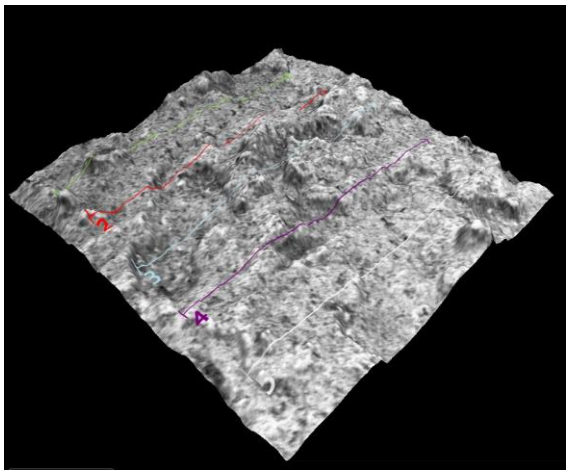

Fig. 11. Surface of a steel sample from a serial collector (3D)

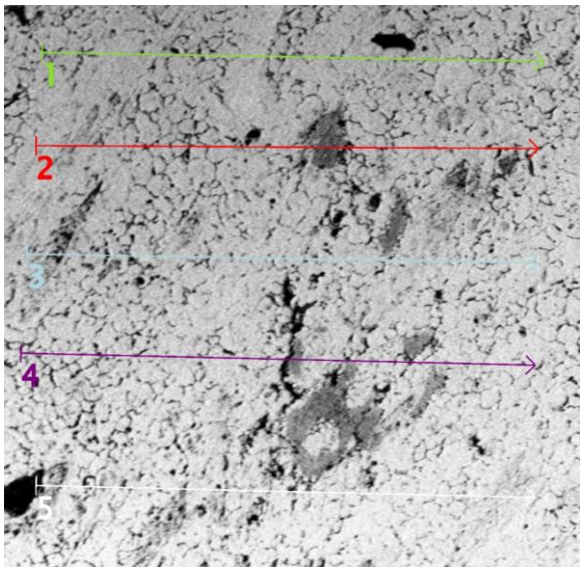

Fig. 12. Surface of a steel sample from a sports collector (2D)

Table 4. Roughness measurement results (series collector)

Area no	Measurement no	R_z [µm]	R_a [µm]
I	1	23.96	14.50
	2	24.63	12.00
	3	33.18	15.67
	4	16.25	8.21
	5	20.85	9.25
II	1	21.73	10.37
	2	24.27	7.76
	3	26.55	11.26
	4	18.77	8.43
	5	16.23	9.81
II	1	20.20	7.40
	2	23.95	18.24
	3	14.72	5.47
	4	11.29	5.00
	5	9.96	4.32
Mean value [µm]		20.44	9.85

An unique proof of the influence of roughness on flow resistance will be an analysis in which two identical pipes are put together, for which the boundary conditions of the flow will be the same, but will differ in the roughness of the inner surface. Figures 15 and 16 show the simulation results for pipes with a diameter of 49.4 mm and a length of 500 mm. The grid parameterization was carried out for the values used in the previous simulation of the collectors. The material used is steel with the average R_z value of both cases, determined based on the conducted microscopic measurements. The calculations were made for the input velocity Vi = 200 m/s and the number of iterations equal to 1000. The pressure distribution for a pipe with a roughness of R_z = 20.44 µm is shown in Fig. 14. The pressure differences for this case are shown in Fig. 15. The pressure distribution for a pipe with roughness R_z = 9.44 µm are shown in Fig. 16. Pressure differences for this case are shown in Fig. 17.

Table 5. Roughness measurement results (sports collector)

Area no	Measurment no	R_z [µm]	R_a [µm]
I	1	12.73	7.65
	2	14.99	7.99
	3	7.93	4.23
	4	6.51	4.45
	5	6.32	4.58
II	1	9.69	4.07
	2	6.32	5.68
	3	8.58	4.90
	4	6.70	2.86
	5	6.53	6.71
II	1	11.45	3.63
	2	14.18	15.08
	3	7.41	9.13
	4	11.35	9.71
	5	10.94	8.17
Mean value [µm]		9.44	6.59

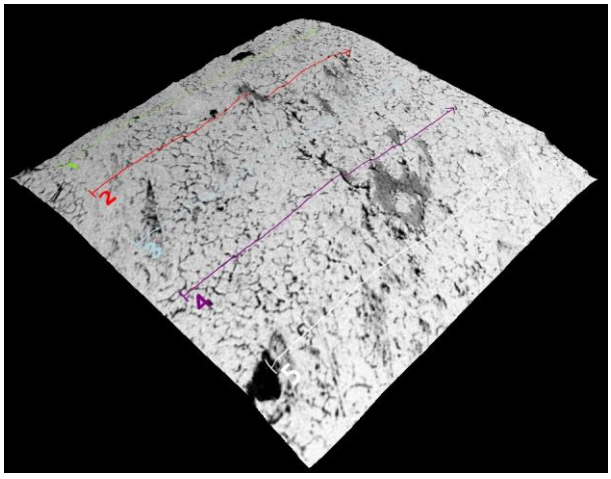

Fig. 13. Surface of a steel sample from a sports collector (3D)

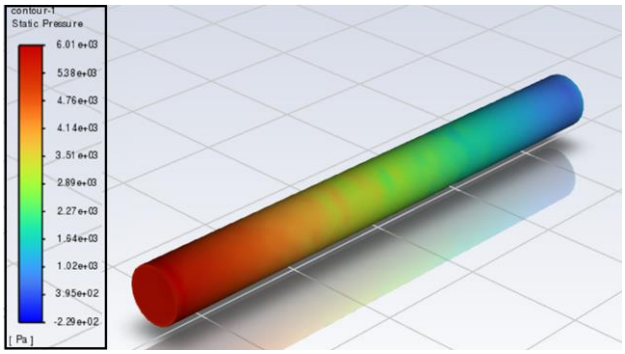

Fig. 14. Pressure distribution in a pipe with roughness R_z = 20.44 µm

Area-Weighted Average Static Pressure	[Pa]
(inlet)	5709.2167
(outlet)	476.26152
Net	3092.7391

Fig. 15. Differential pressure at the inlet and outlet (R_z = 20.44 μm)

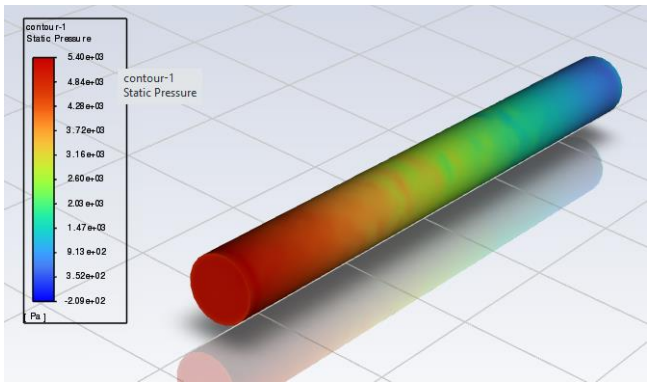

Fig. 16. Pressure distribution in a pipe with roughness R_z = 9.44 μm

Area-Weighted Average Static Pressure	[Pa]
(inlet)	5099.9846
(outlet)	471.78094
Net	2785.8828

Fig. 17. Differential pressure at the inlet and outlet (R_z = 9.44 μm)

Comparing the calculation results for both pipes, we can observe the pressure difference at the inlet and outlet of the pipe. In the case of a pipe with a greater roughness, the pressure drop between the beginning and the end of the pipe is 5233 Pa, while in the case of the second pipe this value is 4628 Pa. The summary shows the influence of surface irregularities on flow resistance, which in the analysis, where the only lack of identity between the parameters is roughness, will be manifested in the pressure drop along the length of the pipe.

6. Modification of the exhaust system

Compared with the standard equipment, the system was almost completely modified, starting with the replacement of collectors (Fig. 18), and the replacement of catalysts (Fig. 19), which, in combination with the previously mentioned collectors, are to guarantee the increases declared by the manufacturer. Going further in the system, the pipes are joined in the shape of the letter "X" (Fig. 20), which is to ensure effective pressure equalization between the two columns of flowing flue gases. At the very end of the system there is a final silencer, which has not changed. The selected design solutions resulted in the removal of two middle silencers, which will certainly increase the noise level but should also be used to reduce flow resistance. The view of the entire exhaust system is shown in Fig. 21.

Fig. 18. Sports collectors used in the tested object [20]

Fig. 19. Sports catalysts used in the test object [20]

Fig. 20. X-pipe connector

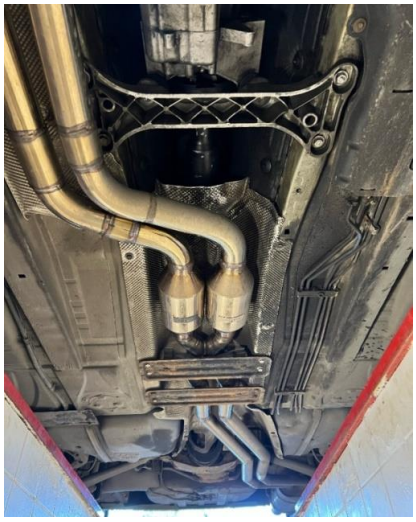

Fig. 21. The entire exhaust system after modification

7. Measurement results

7.1. Testing on a dynamometer before modifications

The first measurement was carried out on gasoline fuel. The measurement results show the curve of engine power, wheel power, torque and power losses. The left vertical axis shows the engine power value. The torque value is on the right vertical axis.

The horizontal axis shows the scale of the engine rotational speed. As you can see in the graph, there are two curves corresponding to the power curve – no. 1 (engine power) and no. 2 (wheel power), the former shows the power generated by the engine, while the second shows the power that the vehicle has in terms of ratio to the wheels, i.e. it takes into account the losses generated by the drive train. The measurement of losses is possible thanks to the dynamometer algorithm, which, after measuring the power on the wheels, is able to take into account the losses generated by the transmission system and convert them into the final result of the power on the engine. In practice, the reading of losses consists in pressing the clutch pedal, after accelerating the engine to the maximum value, which results in disconnecting the gearbox from the shaft of the drive unit. The result will be a reading of the operating characteristics of all drivetrain elements between the engine and the wheels of the vehicle. The loss curve is also shown on the chart (curve no. 3). The measurement results are shown in Fig. 22.

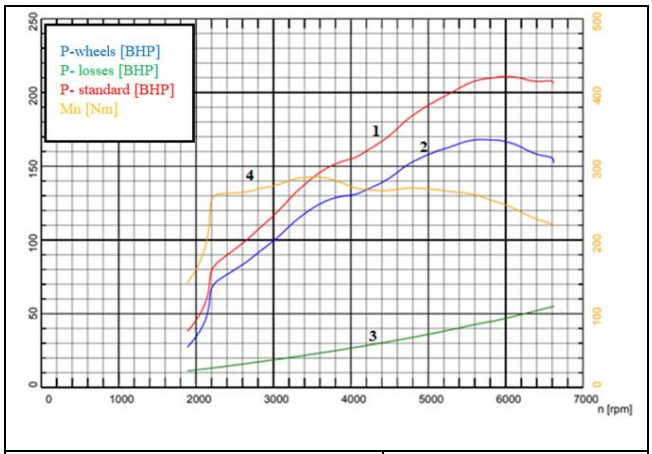

Power measurement parameters		Enviromental parameters	
1 Power according to standards	210.7 BHP/155.0 kW	Ambient temperature	24.0 °C
1 Power on engine	213.5 BHP/15.0 kW	temp. intake air	13.2 °C
2 Power on wheels	166.9 BHP/122.8 kW	Air humidity	55.0 %
3 Power loss	46.5 BHP/34.2 kW	Atmospheric pressure	1014.4 hPa
Maximum power at	5965 rpm/174.3 km/h	Steam pressure	16.4 hPa
4 Torque	285.2 Nm	Oil temperature	–
Maximum torque at	3525 rpm/103.0 km/h	Fuel temperature	–
Max. achieved rotational speed	6620 rpm/193.2 km/h		
[1)] Correlation by DIN 70020			
Correlation coefficient Q_v = 0%			

Fig. 22. Power characteristics of the engine with the factory exhaust system

The maximum power of the engine was 210.7 HP, which differs from the declared catalogue value of 231 HP by just over 20 HP, which translates into an approximately 8.7% decrease in power. This difference is probably due to the mileage of the vehicle, which is over 290,000 km. Before the measurement, the engine itself was partially regenerated – valve seals were replaced and the variable valve timing system (Vanos) was regenerated, while the sealing piston rings were left, which may be one of the reasons for the decrease in power. Torque peaks at 285.2 Nm at an engine speed of 3525 rpm and stays close to this value over a wide rev range, resulting in high engine flexibility between 2100 and 5000 rpm. Maintaining this rpm range will result in the most effective acceleration of the vehicle and the most efficient hill climbing. The maximum value of the torque declared by the manufacturer is 300 Nm, which in relation to the value generated by the tested vehicle gives a decrease of 5%. Comparing this value to the decrease in power, which is the product of torque and engine speed, with its highest value in the upper range of revolutions (i.e. 5965 rpm), it can be concluded that the losses caused by the vehicle mileage increase with the increase in engine speed. The engine operating at high load (high-speed range) due to the high pressure generated in the cylinder, creates favorable conditions for generating high losses caused by poor sealing of the combustion chamber, which in a way may be a good justification for earlier predictions of the reasons for power drops.

7.2. Testing on the dynamometer after modification

After modifications, the maximum engine power reached 231.9 HP for an engine speed of 5740 rpm. The torque curve, after exceeding 2050 rpm, remains close to the maximum level, while it reaches its peak at a rotational speed of 3475 rpm, for which it takes the value of 317.3 Nm. The torque characteristic illustrates the flexibility of the engine in which range it will most effectively accelerate and climb hills, this range starts at 2050 rpm and ends at 5000 rpm. After reaching this value, the curve assumes lower and lower torque values as the engine speed increases. The measurement results are shown in Fig. 23.

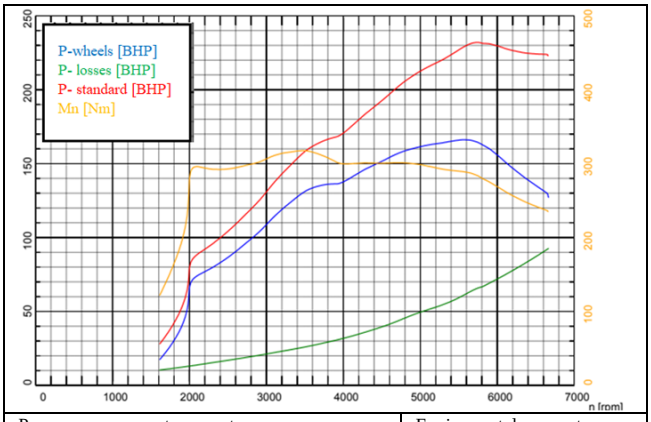

Power measurement parameters		Enviromental parameters	
Power according to standards	231.9 BHP/170.5 kW	Ambient temperature	22.7 °C
Power on engine	230.0 BHP/169.1 kW	temp. intake air	14.7 °C
Power on wheels	164.3 BHP/120.9 kW	Air humidity	28.2 %
Power loss	65.6 BHP/48.3 kW	Atmospheric pressure	995.6 hPa
Maximum power at	5740 rpm/199.7 km/h	Steam pressure	7.8 hPa
Torque	317.3 Nm	Oil temperature	–
Maximum torque at	3475 rpm/120.9 km/h	Fuel temperature	–
Max. achieved rotational speed	6665 rpm/231 km/h		
[1)] Correlation by DIN 70020			
Correlation coefficient Q_v = 0%			

Fig. 23. Engine power characteristics after modifications

7.3. Comparison of dyno measurements bed

Figure 24 shows a summary of the measurement results, before and after the modification, comparing both runs, an increase in the maximum values of engine power and torque can be seen. The power curve after the modification is almost uniform until it reaches around 3500 rpm. After exceeding this value, the power begins to take higher values for the same rotational speed as before replacing the exhaust system. Referring to the maximum values in both measurements – the power increased by 21.2 HP, which gives an increase of 10% of the power before the modification. Comparing the courses of the torque curves, it can be seen that above the value of 2250 rpm, the measurement made after the modification reaches higher torque values over all the graph. And the maximum value increased by 32 Nm and this way ensured an increase of 11%.

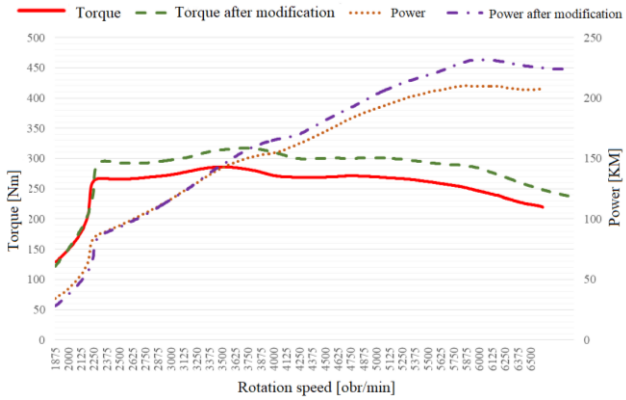

Fig. 24. Comparison of the results of both measurements

8. Conclusions

Comparing the computational models of both collectors, the first observation that comes to mind is the difference in pressure distribution. Exhaust gases flowing through the serial collector generate a very non uniform pressure distribution inside the ducts, while the sports collector outside individual zones is characterized by a stable level of gas pressure on the walls throughout its volume. Such a state of flow parameters will certainly be more advantageous, taking into account for example the uniformity of wear of individual fragments of the tested element. The analysis did not take into account the temperature distribution in individual sections, but local pressure increases can certainly increase the thermal impact, which may result in dangerous heating of the collector. High temperature on the uninsulated manifold can adversely affect the performance of the drive unit due to the lack of additional heat dissipation from the engine compartment. On the other side considering the effect of this phenomena, some benefits can be find in high temperature of the flue gases entering the catalyst, which will increase the efficiency of the reactor in the catalysis process. In the case of a sports manifold, the flowing exhaust gases will not influence on temperature inside the engine compartment, and the structure itself will be less strained due to the even distribution of forces in individual channels. The other expected benefit of the method of routing the pipes in the modified system, apart from the uniform distribution of stresses, will be the distance to which the channels coming out of the engine block are led out. This solution is rationally justified by the distribution of the energy of the escaping gas over a larger surface and the resulting discharge of excessive temperature outside the engine chamber. Considering condition of the surface of both collectors and its impact on the free flow of gas (referring to the roughness analysis), it can be concluded that the low roughness of the modified system and the stable pressure distribution will have a more beneficial effect on reducing the resistance to movement of the flowing exhaust gases, and thus their more effective discharge.

The measurement power after the modification successfully confirmed the hypothesis of the possibility of increasing engine performance by interfering with the exhaust system only. The comparison of both characteristics in one coordinate system shows the impact of modifications on the increments of operational parameters. A very satisfactory effect is the translation of the torque curve along the Y axis, what gives the possibility of having higher acceleration of the vehicle in the same engine speed range as before the modification. This modification is clearly felt during drive, especially when the gearbox is overvoltage in third gear, the vehicle has a very efficient acceleration ability in this respect. Analyzing the course of the power curve, it can be seen that after the modification it is almost the same, but after exceeding the barrier of about 3500 rpm, it takes on higher values. The increase in power can also be defined on the basis of the maximum engine speed achieved, for which the vehicle speed increased by 38.6 km/h. Changes in the achieved maximum parameters of the engine are most consistent with the increases declared by the manufacturer, probably in the case of a unit with a lower mileage and less wear of individual components, the impact of the modification would be even more effective, which would additionally confirm the effectiveness of the exhaust system used.

The comparison of individual construction solutions and the physical benefits resulting from them in relation to the unit measurement of output parameters is a very risky move. The study shows the change in the power and torque curve under the influence of modifications to the design of one engine with specific initial parameters. And it is difficult to systematize the reason of individual increases in a more universal nature. But based on the knowledge of people experienced in this field who had the opportunity to observe the impact of individual modifications on the formation of torque and power curves, one can attempt to correlate certain phenomena. One of them is the use of collectors with a higher flow capacity, which could increase the torque.

According to the opinion of experienced mechanic engineers, the result of such a change is having higher torque at an earlier stage of engine speed. The above statement is justified by the results of the tests, observing the course of the torque. It reaches values close to the maximum at 2200 rpm already, whereas before the modification such values could be observed for a rotational speed of about 3500 rpm. Potential correlations can also be found in the use of sports catalytic converters. Their metallic filling (providing less resistance) and a smaller number of channels guarantee better exhaust gas flows in comparison with classic catalyt-

ic reactors with ceramic filling, which concerning the engine's output parameters, are supposed to increase the maximum power. The measurement after the modification clearly indicates the possibility increasing the power by as much as 21 HP. But this merit should not be attributed only to this solution. The system was completed by one manufacturer who had previously calculated the efficiency of his set and probably the power increase would not have reached such values without interfering with the construction of the collector. The remaining parts of the system, despite occurrence of favorable physical phenomena during the exhaust gas flow, will have a rather marginal impact on the formation of the engine output parameters and can be classified as a complement to the effectively constructed system. Fragments of this type are used in the tested object: X-pipe type connector and pipes with relatively low roughness, made of 304 stainless steel. The effect of the modification, apart from increasing engine parameters, are also other usable aspects, such as increased noise emission. The vehicle was tested with unprofessional measuring equipment in the form of a mobile application, where the result before the replacement was 100 dB, and after the modification it reached the value of 112 dB. The reason for the increase in noise emissions was undoubtedly the removal of the center mufflers, which could also be a potential obstacle to maximizing the vehicle's performance.

Acknowledgements

The article was written in cooperation with Autocomp Management Sp. z o.o. from Szczecin, Research and Development Center – producer of simulators on the military and civilian market from Poland.

Nomenclature

BHP	brake horsepower
CFD	computational fluid dynamics
DSC	dynamic stability control
Ra	roughness average
Rz	mean roughness depth

Bibliography

[1] ANSYS. ANSYS-Fluent-Tutorial-Guide_r170.pdf.
[2] ANSYS. ANSYS Meshing User's Guide_r130.pdf. ANSYS 2013.
[3] Allawi MKA, Oudah MH, Mejbel M. Analysis of exhaust manifold of spark-ignition engine by using computational fluid dynamics (CFD). Journal of Mechanical Engineering Research and Developments. 2019;42(5). https://doi.org/10.26480/jmerd.05.2019.211.215
[4] Chandak A. Investigation and design modification in exhaust manifold. SSRN Electronic Journal. 2020:6. https://doi.org/10.2139/ssrn.3524751
[5] Cho K-S, Son K-B, Kim U-K. Design of exhaust manifold for pulse converters considering fatigue strength due to vibration. Journal of the Korean Society of Marine Engineering. 2013; 37(7):694-700. https://doi.org/10.5916/jkosme.2013.37.7.694
[6] Detailed drawing and dimensioning – auxiliary materials. Gdynia Maritime University. http://wm.umg.edu.pl/cwiczenia/grafika/oznaczanie_chropowatosci_materaily_pomocnicze.pdf
[7] FLUENT User's Guide. ANSYS 2013.
[8] Hessamedin N, Davood DG, Mofid G, Ghasem J, Mojtaba K. A parametric design of compact exhaust manifold junction in heavy duty diesel engine using computational fluid dynamics codes. Thermal Science. 2011;15(4):1023-1033. https://doi.org/10.2298/TSCI100417041N
[9] Han-Chi H, Hong-Wu H, Yi-Jie B. Optimization of intake and exhaust system for FSAE car based on orthogonal array testing. International Journal of Engineering and Technology. 2012;2(3). https://www.semanticscholar.org/paper/Optimization-of-Intake-and-Exhaust-System-for-FSAE-Han-chi-Hong-wu/7279378088fff0ad35490a4c904214449f67e65b
[10] Hasan JM, Mohammad WS, Mohamed TA, Alawee WH. CFD simulation for manifold with tapered longitudinal section. International Journal of Emerging Technology and Advanced Engineering. 2014;4(2):28-35. www.ijetae.com
[11] Kanawade N, Siras O. A literature review on exhaust manifold design. International Journal of Scientific Research Engineering & Technology. 2016;5(5). www.ijsret.org
[12] Kordziński C. Exhaust systems of high-speed internal combustion engines. WKL. Warsaw 1964.
[13] Kowalewski A. Exhaust systems. Construction, tasks, requirements; update date: 2016.10.21.
[14] Kordziński C. Increasing engine performance for cars and motorcycles. WKL. Warsaw 1964.
[15] Krishnara JC, Rajesh Ruban S, Subramani N. Analysis of exhaust manifold to improve the engine performance. International Journal of Engineering & Technology. 2018;7(2.8): 539-542. https://doi.org/10.14419/ijet.v7i2.8.10517
[16] LPS 3000 – chassis dynamometer. Original instructions for use BA052301-pl.
[17] Mączyński J. Fluid mechanics. National Scientific Publishing House. Warsaw 1966.
[18] Muchhetti M, Suman DS, Abhiman B, Madhukar S. Design and analysis of X shaped exhaust system operation using different types of profiles on high capacity vehicle. International Journal of Scientific Research in Science, Engineering and Technology. 2021;8(4):19-27. https://doi.org/10.32628/IJSRSET218411
[19] Parts catalog of original parts BMW. www.realoem.com/bmw (accessed on 17.04.2023).
[20] Schmiedmann online store. www.schmiedmann.com (accessed on 17.04.2023).
[21] Thangapandian P. Design and analysis of exhaust manifold for multicylinder diesel engine with monolith catalytic converter using CFD. International Journal of Applied Science and Engineering. 2022;19(1):1-9. https://doi.org/10.6703/IJASE.202203_19(1).003
[22] Umesh KS, Pravin VK, Rajagopal K. CFD analysis of exhaust manifold of multi-cylinder SI engine to determine optimal geometry for reducing emissions. International Journal of Automobile Engineering Research and Development. 2023;3(4):45-56. http://www.tjprc.org/publishpapers/--1380373503-5.%20CFD%20Analysis.full.pdf

[23] Usan M, Weck O, Whitney D. Exhaust system manifold development enhancement through multi-attribute system design optimization. AIAA 2005-2066. 46th AIAA/ASME/ASCE/AHS/ASC Structures, Structural Dynamics and Materials Conference. April 2005. https://doi.org/10.2514/6.2005-2066

[24] Venkatesan SP, Ganesan S, Devaraj R, Hemanandh J. Design and analysis of exhaust manifold of the spark ignition engine for emission reduction. International Journal of Ambient Energy. 2020;41(6):659-664. https://doi.org/10.1080/01430750.2018.1484811

[25] Zhang X, Luo Y, Wang J. Coupled thermo-fluid-solid analysis of engine exhaust manifold considering welding residual stresses. Transactions of JWRI, 2012:75-77. https://doi.org/10.18910/23075

Bartosz Bober, Eng. – Faculty of Mechanical Engineering, Wroclaw University of Science and Technology, Poland.
e-mail: *bartoszbober383@gmail.com*

Monika Andrych Zalewska, DEng. – Faculty of Mechanical Engineering, Wroclaw University of Science and Technology, Poland.
e-mail: *monika.andrych@pwr.edu.pl*

Piotr Boguś, DSc., DEng. – Head of Department of Physics and Biophysics of Medical University of Gdańsk, Poland.
e-mail: *piotr.bogus@gumed.edu.pl*